Dynamical Resonant Structures in Meteoroid Stream Orbits

R. H. Soja[1,2]⋆, W. J. Baggaley[1]†, P. Brown[3], D. P. Hamilton[4]

[1] *Department of Physics and Astronomy, University of Canterbury, Christchurch, New Zealand*
[2] *European Space Astronomy Centre (ESAC), Villanueva de la Cañada, Madrid, Spain*
[3] *Department of Physics and Astronomy, University of Western Ontario, London, Ontario, Canada*
[4] *Department of Astronomy, University of Maryland, College Park, Maryland, U. S. A.*

Draft 29 Nov 2010

ABSTRACT
Herein we use the Canadian Meteor Orbit Radar (CMOR) dataset to search for evidence of a resonant swarm in the Taurid meteoroid stream at the 7:2 Jovian resonance. We use a numerical method to estimate the reduction in radar orbit measurement uncertainty required to detect this feature in a dataset. This is highly dependent on the proportion of observed particles that are members of the resonant swarm. However, we find that a meteor radar with uncertainties a factor of ten lower than those of the current CMOR will be sufficient for detection to be possible, if the meteor shower consists of more than 5% resonant particles (considered likely given the results of visual meteor studies). Such an improvement will require accurate removal of deceleration errors from pre-atmospheric meteor velocities, and improvement to the robustness of echo inflection point identification algorithms and interferometric measurements.

Key words: meteorites, meteors, meteoroids – comets:individual:2P/Encke.

1 INTRODUCTION

Meteoroid particles ejected from cometary or asteroidal parent bodies are subject to gravitational and nongravitational forces. These act to perturb such particles from their initial orbits, and eventually may cause their removal from the Solar System by collision with an additional body or by expulsion from the Solar System. Non-gravitational forces include radiation pressure, Poynting-Robertson and solar wind drag forces, and magnetic field effects. Gravitational effects include direct perturbations caused by planetary bodies, and resonance effects, generally of Jupiter or Saturn, but theoretically also as a result of any large body in the Solar System.

As well as causing dispersal of particles, such resonances are able to concentrate or protect bodies at specific locations. Resonant swarms can be formed as a result of the ejection of particles by a resonant or near-resonant comet. Particles injected into the stream by the parent comet each have slightly different orbits, with a small proportion having the correct dynamics to place them inside a resonance, particularly if the comet already librates within a given resonance. These particles can remain in this region for relatively long periods of time, their existence inside the resonance (or near a librating comet) protecting them from planetary perturbations and other such effects that act to more quickly disperse other stream particles. Inside the resonance, these particles are concentrated in a narrow range of mean motions, thus producing enhanced shower flux at the Earth when the displacement between the Earth's position and the resonance centre is small. Built up over a number of comet returns to the resonance centres, these regions have relatively high particle density, and are wider than outburst dust created by dust trails from a single comet pass. These dust trails produce outbursts because the particles are young and have not had sufficient time to disperse into the stream background. It is important to distinguish between relatively old, wider resonant swarms or filaments injected into the region over a number of years, and young dust trails of recently released material.

A resonant swarm at the 7:2 Jovian resonance in the Taurid meteoroid stream was proposed and described by Asher, Clube and Steel (1993). This paper also examined records of elevated Taurid meteor observations from 1931 to 1988, and found five occasions that have $|\Delta M|$ less than $40°$ (where, ΔM is the displacement in mean anomaly of the resonant centre from the point at which the Earth and swarm orbits cross in space and time), suggesting a potential link. The nearby 3:1, 4:1, 10:3 and 11:3 Jovian reso-

⋆ E-mail: rachel.soja@sciops.esa.int (RHS)
† E-mail: jack.baggaley@canterbury.ac.nz (WJB)

nances were found incapable of matching these observations. The authors construct a table of predicted years ('swarm-encounter' years) in which the swarm may be observed on Earth: these are years for which $|\Delta M| \leqslant 40°$.

Observational evidence in support of the existance of this stream is given by Asher and Izumi (1998), Beech, Hargove and Brown (2004) and Dubietis and Arlt (2007). This swarm theory was proposed in conjunction with the fragmentation of a 'giant' proto-Encke comet over the past $\sim 2 \times 10^4$ years, which may have inhabited a resonant orbit for a fraction of its lifetime (Asher and Clube (1998). A concentration of particles in a resonant swarm at the 7:2 resonance is possible even without the existance of such an object. However, formation of a resonant swarm is more difficult without a resonant or near resonant parent object.

It may be possible to observe this swarm in meteor radar orbit data. Below we demonstrate that the Taurid swarm is expected to be among the most easily-observed resonance effects in radar data. It is expected that the size of the swarm and the measurement uncertainties of the radar will limit the observability of the swarm. In this paper we investigate these limitations to develop an understanding of the capability of radar techniques in discerning resonant swarms.

2   THE CANADIAN METEOR ORBIT RADAR

Canadian Meteor Orbit Radar (CMOR) data is used to study the observability of resonance features in meteor orbit radar. This is a three-station pulsed meteor radar operated by the meteor group at the Department of Physics and Astronomy, University of Western Ontario, London, Canada. Situated near Tavistock, Ontario, Canada (80.772°W, 43.364°N), it has two remote sites 8.1km and 6.2km from the central site. The three stations form an angle of 96.8°. It is a SKYiMet radar system (see Hocking et al. (2001)) with a peak power of 6.0 kW capable of three frequencies (17.45, 29.85 and 38.15 MHz). A five-element interferometer allows determination of echo directions to $\sim 1°$ (above 20° elevation). CMOR uses vertically directed arrays resulting in almost all-sky coverage down to $\sim 20°$ elevation. A pulse repetition frequency of 532 Hz and a pulse length of 75 μs are used. Radiant directions have an uncertainty $\sim 6°$ (due to the uncertainty in the measurement of time-delays). Further details are available in Jones et al. (2005).

CMOR meteor velocities are determined using multi-station timing. Errors in time inflection picks are roughly 0.7 of the interpulse time, corresponding to errors of order 1.3 ms. This time inflection pick error dominates the error in the final velocity, which is of order 10%. A pre-t_0 Fresnel oscillation method is used to provide speeds with uncertainties $\sim 5\%$ for approximately 10% of meteors that have high signal-to-noise Fresnel patterns (Hocking 2000). Deceleration corrections are computed using empirical expressions determined by comparing the raw radar-determined speeds with the speeds found in photographic studies of major meteor showers (Brown et al. 2004).

3   RESONANT SWARMS IN METEOROID STREAMS

Here we evaluate which meteor streams are most likely to provide evidence of resonant effects in meteor orbit radar data. This will provide the most promising stream candidate for study in the current dataset. Meteoroid streams in which resonant effects have been observed include the Quadrantids, Perseids, Leonids, Orionids, June Bootids, Lyrids, Ursids, and Taurids (see Jenniskens et al. (1998); Jenniskens & Betlem (2000); (Emel'yanenko 2001a); Asher & Emel'yanenko (2002); Sato & Watanabe (2007); Trigo-Rodríguez et al. (2007); Rendtel (2008); Spurný & Shrbený (2008)). From the analytic study of Emel'yanenko (2001a), the Perseids, Eta Aquarids, Orionids, Lyrids, Leonids, and June Bootids have dynamics that may allow stable swarms to form at resonance locations. Ryabova (2005) also notes that the Geminid stream may contain a resonant concentration due to its close proximity to the narrow 7:1 and 8:1 resonance regions.

To evaluate the observability of resonance effects in these streams in CMOR data we consider, the position of the radiant of the corresponding meteor shower, the velocity of incoming meteors, the zenith hourly rate, and the resonance width. The radiant declination will determine whether a radar system at a given latitude can observe the shower. The velocity is used to determine semi-major axis values for the particle orbits, but most importantly is indicative of the relative uncertainties: observational radar uncertainties increase as the geocentric velocity of the particle increases, and are dependent on the relative impact geometry with the Earth, being greater for head-on collision. Therefore, high Earth-impact velocities can increase the difficulty of observing small-scale structure in the semi-major axis. The zenith hourly rate (ZHR) is the number of meteors expected to be observed per hour on a clear, moonless night with the shower radiant at the zenith (Murad & Williams 2002). This parameter can be used as a relative measure of meteor shower strengths: showers of higher ZHR are more likely to produce statistics sufficient to overcome large measurement uncertainties. However, ZHR values are usually based on visual observations, and are not always representative of the shower rates at the radar mass level. Therefore, here we instead use the 'maxZ' parameter defined in Brown et al. (2008) as 'the relative activity strength at maximum' (Brown et al. 2008). The resonance width will determine if a resonant feature is important with respect to uncertainties: a very small resonant width compared with measurement uncertainties will make detection difficult as the uncertainties will restrict the ability to sense small-scale features.

Table 1 summarises approximate values for the above parameters for the showers of interest. All of the showers are within the observing limits for CMOR, having declinations greater than $\sim -20°$. The effect of different impact velocities (V_g) is demonstrated by a representative semi-major axis uncertainty δa at the resonance semi-major axis, which we determine using CMOR data. A useful measure defined here for deciding the potential for observation of resonance effects by radar in a given meteor shower is the ratio of the approximate width of the resonance to this representative δa. The greater the resonant width is in comparison to the uncertainties (thus the higher the ratio), the higher the

Table 1. *Parameters of use in determining the suitability of meteor showers in resonant studies. Dec is the shower mean declination; V_g is the shower mean geocentric velocity, with the associated error as measured by CMOR; a is the shower mean semi-major axis; res is the known or theorised (marked with ?) Jovian resonance in which shower particles are involved; a_R is the approximate semi-major axis location of the resonance; width is the approximate resonant width, generally taken from (Emel'yanenko 2001b); δa is the range of uncertainties in CMOR semi-major axis values at a; maxZ is the relative activity strength at maximum (an instrumentally-biased proxy for a ZHR-like measure of strength); and ratio is the ratio between the resonant width and δa (a measure of the how appropriate the shower is for radar resonance studies)*

Shower	Dec	V_g	$a_{(AU)}$	res	$aR_{(AU)}$	width$_{(AU)}$	$\delta a_{(AU)}$	maxZ	ratio
Quadrantids	+48.5	42 ± 4	3.14	2 : 1	3.28	0.17	1.5–3.5	238	0.11
Perseids	+56.9	62.1 ± 7.2	~ 25	1 : 11	25.7	1.4	128–230	103	0.011
Leonids	+21.6	69 ± 6.8	9.8	5 : 14	10.3	0.13	20–38	82	0.0065
Orionids	+15.5	66.4 ± 6.3	18	1 : 6?	17.2	1.0	55–105	132	0.018
Eta Aquarids	−0.7	64.6 ± 6.2	16.16	1 : 5?	15.2	0.9	45–80	277	0.020
Lyrids	+32.6	47.3 ± 4.1	45.7	1 : 12?	27.3	1.8	140–260	36	0.013
N Taurids	+21.0	28.1 ± 2.9	2.12	7 : 2	2.25	0.05	0.6–1.6	31	0.083
S Taurids	+8.0	27.9 ± 3.7	2.07	7 : 2	2.25	0.05	0.6–1.6	56	0.083
Geminids	+32.1	35 ± 3.8	1.37	7 : 1	1.42	0.006	0.17–0.57	817	0.036
Ursids	+74.6	37.6 ± 5.1	4.62	6 : 7	5.76	0.09	5.5–11.57	29	0.016

chance that the resonant feature will be discernable above the uncertainty broadening of the radar data. These values are also given in Table 1. Indeed, a resonant feature that is too wide will blend easily into the background dust cloud. Thus a relatively low resonant width, but a high ratio of resonant width to semi-major axis uncertainty is preferred. We find the best showers (in order), chosen for their relatively high ratio, are the Quadrantids, Taurids, and Geminids.

We choose the Taurids for continued study due to the lack of observational support for resonant effects in the Geminids, and the large radar meteor uncertainties that will result from the larger velocities and semi-major axis values of the Quadrantids. The observational evidence in visual meteor data for the Taurid swarm at the 7:2 Jovian resonance and the relatively low uncertainties in Taurid velocities and semi-major axes make the Taurid 7:2 resonant swarm a good candidate for a radar search.

4 THE TAURID METEOR COMPLEX

The Taurids are a Northern Hemisphere meteor shower observed in October-November. Commonly, the shower is defined by the Northern and Southern Taurid branches. These are both part of a wider Taurid Complex, to which a number of asteroids have been associated. The 'Giant Comet' hypothesis was formed partially to account for the presence of these objects (Clube & Napier 1984) (Asher et al. 1993): however, the apparent asteroidal nature of many Taurid complex bodies puts this hypothesis in doubt (Jenniskens 2006). Additionally, Valsecchi et al. (1995) found that a dynamical mechanism involving secular resonances is able to transport bodies from the asteroid belt to the Taurid region, though such a process requires a long timescale.

The potential resonant concentration of particles at the 7:2 Jovian resonance is usually investigated using a time-based approach where the years in which the resonant swarm should be visible are calculated. Here, however, we seek evidence for the swarm in the semi-major axis distribution. A possible detection of the swarm in semi-major axis data

is given in Steel et al. (1991). Furthermore, there are insufficient years of CMOR data to search for a evidence for increased Taurid rates in swarm years. Orbital element data only encompasses one swarm-encounter year (2005). Single-station data is available for more years, but this would not allow extraction of Taurid particles from the dataset, as a received signal from at least three stations is required for an orbit to be calculated. Additionally, despite the presence of stronger resonances in the Taurid vicinity (such as the 3:1 and 4:1 Jovian resonances), only the 7:2 resonance is studied because Asher & Clube (1993) find that only this resonance can explain the observed yearly rates of Taurid meteoroids.

As for Kirkwood gaps, resonant effects should be evident as a peak around the location of the 7:2 resonance at a semi-major axis $a = 2.256$ AU. Here a number of methods are employed to attempt to extract evidence of this resonant swarm in CMOR radar data.

4.1 Extracting Taurid Data

We extract Taurid from the CMOR orbital datasets (of the meteor group at the University of Western Ontario, London, Canada) 2002–2007 using solar longitude limits, right ascension and declination, and velocity specifications for the shower in CMOR data (Brown et al. 2008). This resulted in separate datasets of Northern and Southern Taurids, of 1617 and 6032 meteoroids respectively. These are combined here, unless otherwise stated.

Given that the extended Taurid stream encompasses showers either side of the Northern and Southern Taurids, and also in June each year, additional resonance information may be acquired by extension of the dataset to include these showers. However, here we extract only Northern and Southern Taurids as determined by the previous CMOR shower survey of Brown et al. (2008).

Though only the CMOR dataset is examined here, the techniques developed in this work are applicable to the general problem, and can be used to investigate whether evidence exists for any dynamical feature in meteoroid streams

in any radar dataset. Our purpose here is, in addition to searching for evidence of the 7:2 Taurid swarm, to establish a procedure for tackling searches for small-scale structure in radar meteoroid stream data.

5   THE RESONANT WIDTH OF THE 7:2 JOVIAN RESONANCE

Here we determine the resonant width, or size of the region of influence, for the 7:2 Jovian resonance at Taurid orbital elements. This is important here as such knowledge aids in the search for this resonance in the dataset; in the confirmation that a particular feature meets resonant feature criterion; and in determining the upper limits on radar sensitivities and orbital resolution that would enable detection of the resonance.

5.1   Definition of the Resonant Width

Broadly, the libration or resonant width describes the influence of the resonance: the variations in orbital elements (particularly semi-major axis) that the resonance can produce; or the extent (again usually in semi-major axis) over which the resonance exerts a significant effect. Values of the width from these two definitions should agree and also match the observed widths of physical resonance features, such as the Kirkwood Gaps in the Asteroid Belt. In many cases it is thus important to determine the resonance width in semi-major axis, as this is closely related to the size of observable resonance features in the Solar System. In this section we assume that the resonance width refers to a semi-major axis interval, unless otherwise stated.

Mathematically, the width can be defined (from the first definition above) as a maximum libration amplitude by considering the librational motion within resonance. Considering a particle at the exact resonance position, the width is then equal to the maximum change in energy or semi-major axis that can occur and still leave the particle in resonance (defined by the presence of libration). Note that this defines a half width, and care must be taken to determine whether a full width (from resonance edge to resonance edge) or half width (from resonance centre to resonance edge) is given by a particular method.

Here we consider two existing methods for determining the width or strength of a given resonance. First, the derivation for an approximate libration width expression is outlined as given in Murray & Dermott (1999): this comprises the purely theoretical standard libration width approximation, valid at low eccentricities. This approximation can be used to give an approximate resonant width. Second, there exists a semi-analytic or numerical method available for determining resonance strength, developed by Tabare Gallardo (Gallardo 2006). Due to the limitations of both methods at high eccentricities, we primarily use a numerical method for this investigation (see Section 5.4).

5.2   An Analytic Resonant Width Expression

An analytic expression for the resonant width is derived by Murray & Dermott (1999). Determination of the resonant width of a given resonance requires both the disturbing function and Lagrange's planetary equations (see Roy (1988) and Murray & Dermott (1999)). A simplification of the disturbing function is required to allow an analytic derivation of an expression for the resonant width: this requires reduction to a circular ($e = 0$), planar (all inclinations zero), restricted case (negligible mass for the inner perturbed body). These restrictions provide simplified equations of motion in orbital elements. Use of a pendulum model to produce an expression for the total energy of the system provides an expression for the resonant width in semi-major axis:

$$\delta a_{max} = \pm \left(\frac{16}{3} \frac{|\mathcal{C}_r|}{n} e^{|j_4|} \right)^{\frac{1}{2}} a. \tag{1}$$

This can be used to directly obtain a resonant width from knowledge of the resonance and the three bodies involved. Orbital elements required are eccentricity e and semi-major axis a. Here n is the mean motion and $\mathcal{C}_r$ describes a strength term, and is given by:

$$\mathcal{C}_r = \frac{\mathcal{G}m'}{na^2a'} f_d(\alpha) = (\frac{m'}{m_c}) n\alpha f_d(\alpha) \tag{2}$$

Here m' is the mass of the outer perturbing body (Jupiter), m_c is the mass of the central body (Sun), $f_d(\alpha)$ is a function of Laplace coefficients describing the direct terms of the expansion of the disturbing function, $\alpha = a/a'$, and $\mathcal{G} = n^2 a^3/m_c$ is used.

For first order resonances it is more appropriate to use:

$$\frac{\delta a_{max}}{a} = \pm \left(\frac{16}{3} \frac{|\mathcal{C}_r|}{n} e \right)^{\frac{1}{2}} \left(1 + \frac{1}{27j_2^2 e^3} \frac{|\mathcal{C}_r|}{n} \right)^{\frac{1}{2}} - \frac{2}{9j_2 e} \frac{|\mathcal{C}_r|}{n} \tag{3}$$

These expressions are valid for orbits with low eccentricities (eccentricity less than ~ 0.3) and low inclinations, and are only easily computable for resonances for which the product $\alpha f_d(\alpha)$ is easily obtainable. These values are given for certain first and second order interior resonances in Chapter 8 of Murray & Dermott (1999). These include the 2:1, 3:2, 4:3, 3:1, 5:3 resonances, but not the 7:2 resonance.
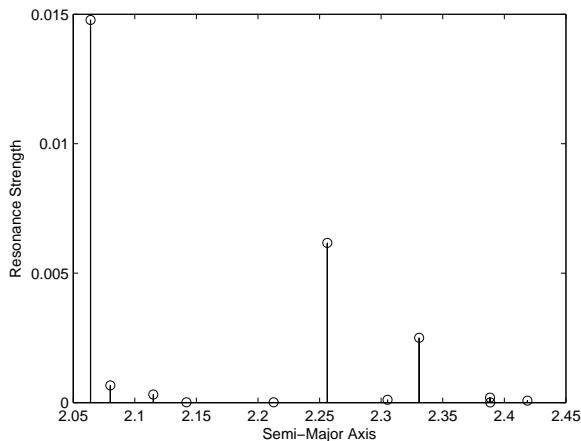
5.3   The semi-analytic resonance strength program of Gallardo (2006)

The semi-analytic method of Gallardo (2006) evaluates the disturbing function $R(\sigma)$ numerically, and then calculates a resonance strength $SR(a, e, i, \omega) = \langle R \rangle - R_{min}$, where $\langle R \rangle$ is the mean value of $R(\sigma)$ with respect to σ (equivalent to the resonant argument φ), and R_{min} is the minimum value of $R(\sigma)$. These resonance strengths are notably different from the other methods in that they are expressed in energy units with $k^2 m = 1$, k being the Gaussian constant of gravity. In order to compare these values to semi-major axis resonant widths of other methods, we must convert SR in energy units to a semi major axis width. Here we derive this conversion using the expression for the expansion of the disturbing function for the circular, planar restricted problem as given by Murray & Dermott (1999):

$$\langle \mathcal{R} \rangle = \frac{\mathcal{G}m'}{a'} [f_{s,1}(\alpha)e^2 + f_d(\alpha)e^{|j_4|} \cos \varphi]$$

where

$$\varphi = j_1 \lambda' + j_2 \lambda + j_4 \varpi.$$

Figure 1. Resonant strengths as calculated for Taurid orbital elements e, i and ω from the amplitude of the disturbing function using $SR(e, i, \omega) = \langle R(\sigma) \rangle - R_{min}$ using numerical techniques and programs developed by Gallardo (2006)

This is simplified using $\mathcal{C}_r$ as given in equation 2 and:

$$\mathcal{C}_s = \frac{\mathcal{G}m'}{na^2a'}f_{s,1}(\alpha) = (\frac{m'}{m_c})n\alpha f_{s,1}(\alpha)$$

This simplification produces:

$$\langle \mathcal{R} \rangle = \mathcal{C}_s na^2 e^2 + \mathcal{C}_r na^2 e^{|j_4|} \cos\varphi$$

Gallardo's resonant strength is the amplitude of the disturbing function $R(\sigma)$. Murray and Dermott's expression is a simple cosine function with amplitude $\mathcal{C}_r na^2 e^{|j_4|}$, so that we find:

$$SR_{approx} = \mathcal{C}_r na^2 e^{|j_4|}. \tag{4}$$

By substituting this into the expression for δa_{max} (equation 1) we obtain an expression for the resonant width as a function of Gallardo's resonant strength:

$$\delta a_{max} = \pm \left(\frac{16}{3} \frac{SR_{approx}a^3}{GM_\odot} \right)^{\frac{1}{2}} \tag{5}$$

Here the mean motion expression $n = \sqrt{\frac{\mu}{a^3}}$ is also used, where $\mu = GM_\odot$. Similarly, for first order resonances we obtain:
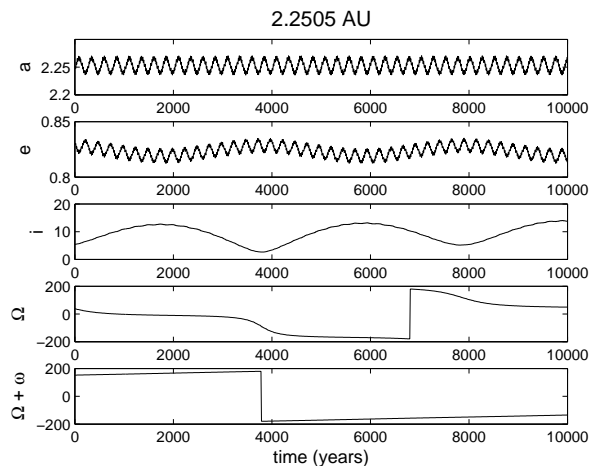
$$\frac{\delta a_{max}}{a} = \pm \left(\frac{16}{3} \frac{SR_{approx}}{n^2a^3} \right)^{\frac{1}{2}} \left(1 + \frac{SR_{approx}}{27e^4n^2a^2} \right)^{\frac{1}{2}} + \frac{2SR_{approx}}{e^2n^2a^2} \tag{6}$$

Because this method relies on low eccentricity approximations, it is expected that these conversion formulae will only be valid for eccentricities less than ~ 0.3.

The strengths for Jovian resonances determined using Gallardo's program ATLAS for the region 2-2.5 AU and for Taurid eccentricity, inclination and argument of perihelion are shown in Figure 1.

5.4 A Numerical Width Determination Method

The resonance width can also be determined by simple examination of the dynamics of a body within the resonance over time. This can be accomplished using an integrator such as the Hierarchical N-Body (HNBody) integrator (Rauch &
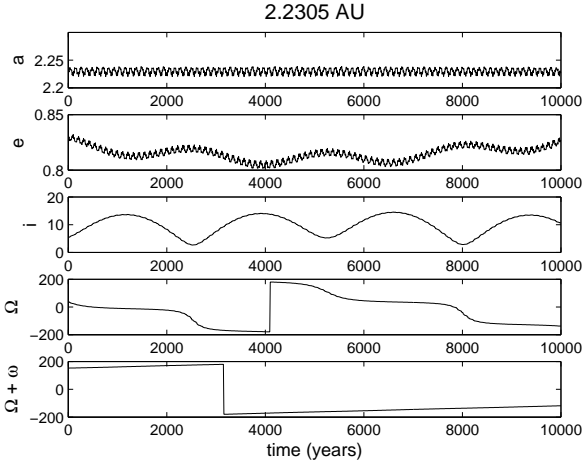
Figure 2. Behaviour of orbital elements over 10^4 year of numerical integration, for particles at Taurid elements $e = 0.83$, $i = 5.4°$, $\Omega = 152.7°$, $\Omega + \omega = 37.3°$, and at $a = 2.2505$ AU. Medium-period resonant oscillations (of period ~ 260 years) and long-term variations are clearly visible.

Hamilton 2002). Here we use HNBody to inject particles into Taurid-like orbits in the vicinity of the 7:2 resonance and study their continuing motions over 10^4 years. The maximum size of oscillations of a particle in resonance provides the resonant width. An additional measure of this width is the size of the region inside which librational motion occurs.

HNBody is appropriate for use in self-gravitating systems with one object dominating the mass of the system, such as is the case for the Solar System. It is primarily a symplectic integrator, but provides Runge-Kutta and Bulirsch-Stoer integrators that are useful in cases where the symplectic integrator cannot provide sufficient accuracy. The Runge-Kutta integrator is most suitable for our problem due to the highly eccentric Taurid orbits.

In our implementation of the meteoroid resonant problem, Sun, Jupiter, and a number of test meteoroid particles are included in the integrations. We find that the exclusion of other planets and asteroids causes negligible error in the resonant width. The meteoroids are given initial orbital elements of Taurid meteoroids, with the exception of the semi-major axis, which is varied slowly between each of the test meteoroids. The Taurid orbital elements used are $e = 0.83$, $i = 5.4°$, $\Omega = 152.7°$, $\Omega + \omega = 37.3°$ (Jenniskens 2006). The mean longitudes of both Jupiter and the particles are zero at present.

We first analyse a region constrained near the 7:2 resonance centre. We present the results obtained for one meteoroid particle in interaction with the Sun and Jupiter. The particle is given a semi-major axis that starts it within the resonance (2.2505 AU). Figure 2 shows the orbital element variations of such a particle over 10^4 years. This particle can be identified as resonant by the relatively long period and large amplitude oscillations visible in semi-major axis (of period ~ 260 years). These oscillations are also present in the eccentricity, superimposed on much longer scale oscillations caused by planetary (Jovian) perturbations (with period ~ 3000 years). Smaller scale variations exist, also the result of predictable Jovian perturbations.
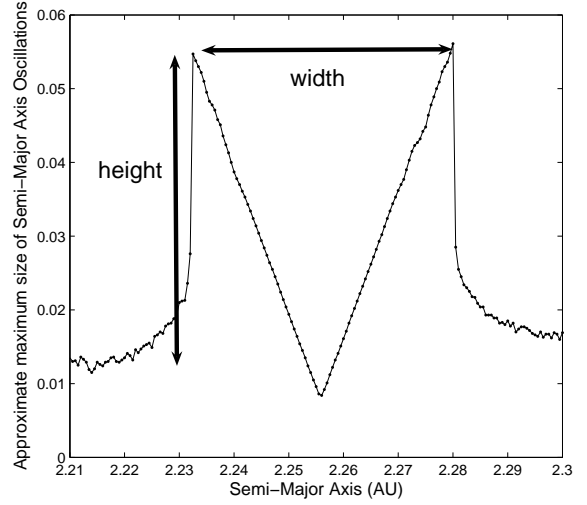
Figure 3. Behaviour of orbital elements over 10^4 year of numerical integration, for particles at Taurid elements $e = 0.83$, $i = 5.4°$, $\Omega = 152.7°$, $\Omega + \omega = 37.3°$, and at (b) $a = 2.22305$ AU. Only longer-term variations are visible (which is outside of the resonance).

A small movement in the starting semi-major axis of the meteoroids (to 2.2305 AU) moves the particle outside the resonance. Figure 3 shows the orbital element variations for this particle: the absence of the large resonant oscillations in the semi-major axis and eccentricity confirms that this particle is not resonant. While the characteristics of semi-major axis oscillations are a good indicator of resonant behaviour, below we use a more rigorous libration test to confirm this.

To examine the semi-major axis oscillations at a variety of positions simultaneously, we analyse a range of particles that scan through the resonance. These provide an indication of the size of the oscillations in semi-major axis over the resonance region (in semi-major axis). We achieve this by stepping through the 7:2 resonance region in steps of 0.0005 AU, with starting semi-major axes of 2.22 to 2.28 AU. The particles are given a mean longitude of 327° and Jupiter a mean longitude of 0. These conditions provide the maximum resonant width, and indicate the approximate location of the resonant centre). For each particle we compute an approximate maximum size for the oscillations in semi-major axis by taking the difference of the maximum and minimum values over the 10^4 year integration. The result is approximately equal to twice the amplitude of the oscillations. This method is limited in accuracy for several reasons, including the presence of long-term variations, but it is found to be sufficiently accurate for our purposes. These approximate 'resonant widths' (as defined in Section 5.1) can be plotted as a function of semi-major axis position to create a pictorial representation of the resonance effects in that region (Figure 4). Figure 5 demonstrates the agreement of the change in the resonant argument (double the libration argument) and the change in the size of semi-major axis oscillations. For the 7:2 resonance at Taurid orbital elements the major libration argument is:

$$\varphi = 7\lambda_J - 2\lambda_P - 5\varpi_P$$

The structure seen in Figure 4 defines a 'resonant feature' that contains valuable information on the dynamics of
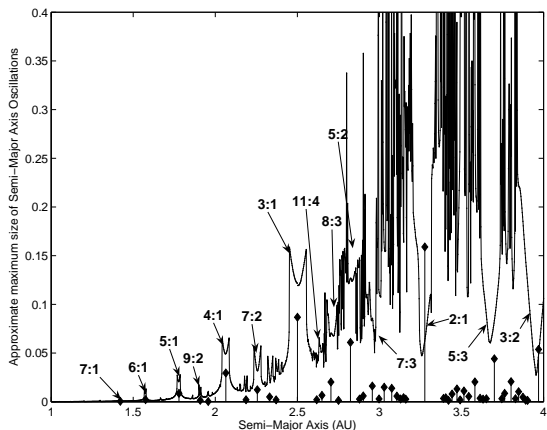

Figure 4. The variation in approximate size of resonant semi-major axis oscillations for particles at starting locations of 2.21 to 2.30 AU. The labels indicate the resonant feature width and height that can both define the width of the resonance.

Figure 5. The variation in approximate size of resonant oscillations for particles at starting locations of 2.22 to 2.92 AU, compared with the variation in the resonant argument. The resonant argument range is equivalent to twice the libration amplitude.

the resonance. The height of this feature gives the maximum size of the oscillations a particle is able to undergo within the resonance. This is similar to the classical definition for resonant width or libration width: the maximum librational motion possible without the particle being lost from the resonance. The width of the feature provides a more physical definition of resonant width: it is the size of the resonant region in which amplified oscillations are present. Furthermore, Figure 5 demonstrates that the dynamics shown by this resonant feature will represent the librational dynamics of the resonance: the area of enhanced semi-major axis oscillations is in agreement with the region in which the libration

Figure 6. The resonance activity at Taurid orbital elements ($e = 0.83$, $i = 5.4$, $\omega = 115.4$) at semi-major axes values 1.0 to 4.0 AU. Gallardo resonant strengths (doubled for visibility) are given by the stem plot below.

Figure 7. Resonant features for the region 2.0–2.5 AU, with a comparison between the case with Jupiter only (crosses), and the case with all planets (dots). Errors in resonant widths are within 0.002 AU.

argument is constrained to a small range of values, and thus the resonant feature well describes the location and extent of the major Jovian resonances in that region.

We find that the width and height of the resonant feature have values (0.047 ± 0.001) AU and (0.047 ± 0.003) AU respectively. We consider the width of the resonant feature to be the more accurate measure of the resonant width as it has a lower uncertainty and is less susceptible to other factors, such as asymmetry of the resonant feature and the definition of the size of small-scale super-imposed perturbations. This is therefore used to give our final resonant width:
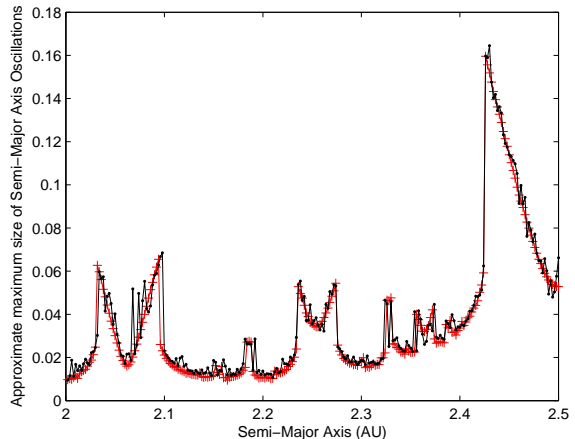
$$(0.047 \pm 0.001)\,\mathrm{AU}$$

The only previous result for the resonant width of the 7:2 resonance at Taurid orbital elements is that given by Asher & Clube (1998), who find that librations are possible between 2.23 and 2.28 AU, implying a libration width of ~ 0.05 AU. Our final resonant width is in good agreement with their result.

5.5 Demonstration of the limited effect of the addition of all planetary bodies

We now use the resonance behaviour in the region 2 to 2.5 AU to demonstrate that only Jupiter significantly affects the width of the 7:2 Taurid resonance. Figure 6 shows the resonant behaviour at Taurid eccentricity and inclination, for orbits with semi-major axis values 1 to 4 AU (the asteroid main belt region). Resonant strengths from Gallardo (2006) are shown for major resonaces to indicate that each resonance feature is present at the expected locations of these major resonances.

The region 2 to 2.5 AU is the 'Taurid region'. Figure 7 shows the resonant behaviour in this region, for integrations for all planets and for Jupiter only. It is evident that little error results from excluding other planets. We ran a similar test including four major asteroids in the Taurid region (Ceres, Pallas, Juno and Vesta), but these bodies produced no significant difference to the distribution of Figure 7.
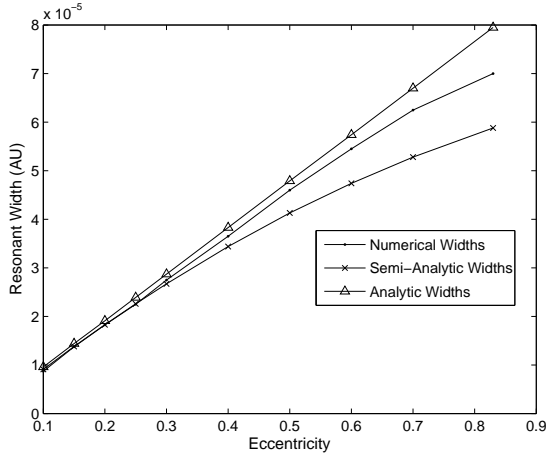
5.6 Comparison of Analytic, Semi-Analytic and Numerical Methods

Here we compare resonant width values (in semi-major axis) given by the three methods outlined in this section. The analytic method is as given in Murray & Dermott (1999): it is derived using a simple pendulum model, and applies in the circular, planar restricted case (see Section 5.2). The semi-analytic method is that developed in Gallardo (2006) (see Section 5.3), which can output a 'strength' for a given resonance, at a given set of orbital elements. The numerical method (see Section 5.4) is the subject of the majority of this work, and involves a numerical determination of the resonant width directly from integrated particle orbits. The purpose of this comparison is to determine the accuracy of the numerical method, and to verify that its results agree with the resonant widths expected by other methods.

The HNBody numerical method we describe here does not include other planetary bodies or radiation effects, though in general it is able to. This method is not, however, restricted by the assumptions of other methods. The analytic approximation requires low eccentricities and zero inclinations, and the Gallardo semi-analytic method assumes that the perturbing planet has zero eccentricity and inclination. HNBody integrations make no orbital element assumptions, and are valid for all orbital elements. Both the analytic and semi-analytic methods deal with an individual resonance, which does not allow for interference effects between different resonances. HNBody considers all gravitational effects of included planets and also includes separate resonant splitting components of the same resonance.

In consequence, there will be intrinsic discrepancies between the brute-force numerical HNBody method and the verification methods, but there should still be a good level of agreement, particularly if HNBody is limited to restrict the differences. In particular, we set the eccentricity and inclination of Jupiter to zero for agreement between the three methods.

The numerical widths used here are the 'width' of each resonant feature. To obtain an accurate width using the
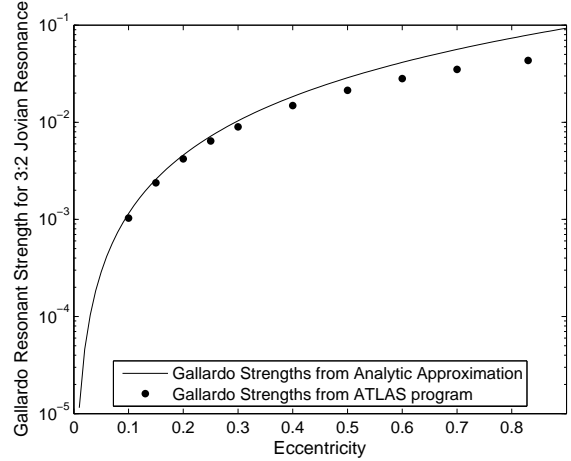
Figure 8. Comparison of numerical resonant widths, analytic widths and semi-analytic widths approximations for the 3:1 resonance at eccentricities 0.1–0.83.

Figure 9. Comparison of 'Gallardo' strengths determined analytically (given by equation 4), and the Gallardo strengths given by the ATLAS program, for the 3:1 Jovian resonance. It can be seen that divergence between the Gallardo strengths given by the ATLAS program, and those determined here from the analytic approximation diverge after an eccentricity of ~ 0.4. The divergence here indicates the error from our conversion of the Gallardo strengths (in energy units) to semi-major axis widths, using equation 5.

above numerical process, we first determine the mean longitudes that describe the resonant centres. These can be estimated using dominant resonant argument equations for each resonance. There will be a small error in this resonant centre due to the presence of resonant splitting terms, but this does not create a large error in the resulting resonant width.
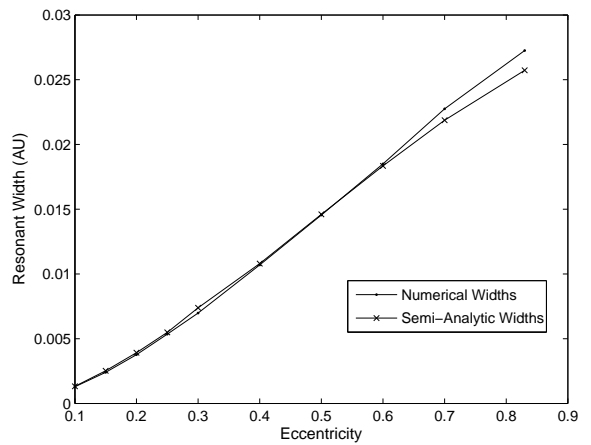
For the analytic case, we use equation 1 to provide direct comparison values. However, its use is expected to be limited to low eccentricities (below values of 0.3) due to the circular orbits assumption inherent in its derivation. To evaluate this equation we require knowledge of the relevant direct term in the expansion of the disturbing function $f_d(\alpha)$. This is difficult to compute, but is given as a product $\alpha f_d(\alpha)$ with $\alpha = a/a'$ for simple first and second order internal resonances in Murray & Dermott (1999). We therefore restrict our comparison to the 2:1 and 3:1 resonances: at an eccentricity of 0.1 for the 2:1 resonance (as high eccentricity orbits in the vicinity of the 2:1 resonance can experience close encounters with Jupiter); and at eccentricities between 0.1 and 0.83 for the 3:1 resonance.

Comparison of the resonant strengths calculated by Gallardo's semi-analytic method with the numerical approach given here requires our conversion of Gallardo's strengths to semi-major axis units (equations 5 and 6). The resulting resonant widths are are only valid for low eccentricity, zero inclination cases as we developed these equations from the circular planar restricted form of the disturbing function given by Murray & Dermott (1999).

Table 2 sumarises the analytic, semi-analytic and numerical widths for the 2:1 resonance. Figure 8 contains the same information for the 3:1 resonance. We divide numerical widths by two in order to give a half width or amplitude that can be directly compared to the analytic and semi-analytic amplitudes. Percentages differences between the methods do not exceed 10% for low eccentricity values $e \leqslant 0.4$. As expected, higher differences between the methods occur at high eccentricities, as a result of the circular assumption used to generate the analytic and semi-analytic equations. This is also illustrated in Figure 9, which shows that the analytic

Figure 10. Comparison of numerical resonant widths and semi-analytic widths approximations for the 4:1 resonance at eccentricities 0.1–0.83.

strength model we derived here (given by equation 4) diverges from Gallardo's resonant strengths after $e \sim 0.4$.

Because the $\alpha f_d(\alpha)$ terms cancel out for the Gallardo width equation, for comparison of the Gallardo method and the numerical method only there is no restriction to only certain simple resonances such as the 3:1 and 2:1 resonances. The 7:2 resonance is not studied here as this is very weak at low eccentricities. Table 10 compares the numerical and Gallardo widths for the 4:1 resonance at various eccentricities. The percentage differences in the methods are less than $\sim 5\%$ for all eccentricities except $e = 0.83$.

We find that the numerical widths do not agree with the analytic and semi-analytic widths within the uncertainties of the numerical width method. This is not unexpected, due

Resonance	Numerical	Analytic	Semi-Analytic	% Variation Analytic	% Variation Semi-Analytic
2:1	0.0635AU	0.0701AU	0.0648AU	-9.4%	-2.0%

Table 2. *Numerical resonant widths, analytic width, and semi-analytic widths approximations for the 2:1 resonance for an eccentricity of $e = 0.1$. Percentage variations are with respect to the numerical widths.*

to the limitations of the various methods, as described at the beginning of this section.

Overall, less than $\sim 10\%$ differences between the numerical widths and the comparison methods are found for eccentricities $e < 0.4$. It is difficult to know what fraction of the variation is from HNBody, and what is fraction is a result of inadequacies of the analytic and semi-analytic approximations. The variation is limited by setting the eccentricity and inclination of Jupiter to zero. Nevertheless, the worst-case scenario is that the differences in the numerical resonant widths are in fact $\sim 10\%$: this can be considered an upper limit for the total inaccuracy of this numerical width method. While the accuracy of the numerical width method is interesting from a theoretical perspective, in this case only an accuracy suitable for application to the meteor orbit radar data is required. Such 10% uncertainties are supportable for this problem: CMOR uncertainties in semi-major axis can be up to ~ 30–40% in individual Taurid orbits.

5.7 Summary

We achieve a numerical value of (0.047 ± 0.001) AU for the width of the 7:2 resonance for Taurid-like orbits. Three methods for determining the resonant width have been found to agree to $\sim 10\%$. This may be considered an upper limit of the error in the numerical width method. It is therefore concluded that the resonant width for the 7:2 resonance for Taurid orbital elements is:

$$(0.047 \pm 0.005)\text{AU}.$$

One benefit of the Gallardo strength program is the computation time: the strengths of a large number of resonances can be calculated to high precision in seconds; while the numerical width method may require tens of minutes to calculate the resonant width (or several hours if several planets are included), and requires use of both HNBody and an additional script to process the output orbital elements. However, the simple numerical width method presented here is capable of determining the importance of resonances at any orbital elements (as is also given by Gallardo (2006)), and additionally provides a physical value which defines the region of influence of the resonance. This numerical width method is thus most useful in the case where information is required on a specific resonance, or in which there is a requirement for a semi-major axis width, as is the situation here. In other situations, the method of Gallardo (2006) may provide a faster approach to analysing the effects of several resonances for objects with high eccentricity or inclination.
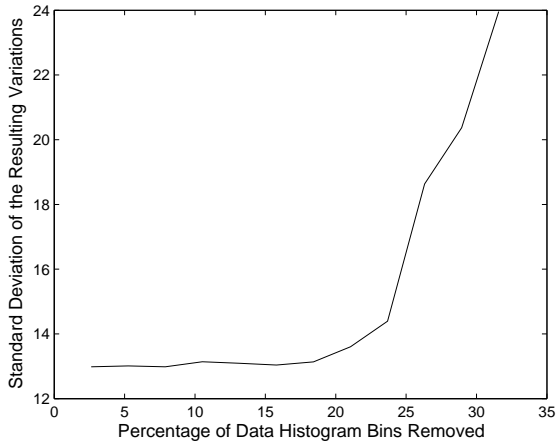
6 STATISTICAL METHODS

In order to investigate the existence of a swarm at the 7:2 Jovian resonance, we conduct a search for evidence of a statistically significant feature at the location of the resonant centre (at $a = 2.25$ AU) in the semi-major axis distribution of the selected Taurid meteoroids. The resonant width determined in Section 5 provides the expected width of the feature in semi-major axis. However, no knowledge is available on the height of the peak the swarm can produce. In Sections 6 to 8 a search for evidence for the resonant swarm in the CMOR Taurid dataset is outlined. Section 9 investigates the effects of radar measurement uncertainties on the ability to detect a resonant feature.

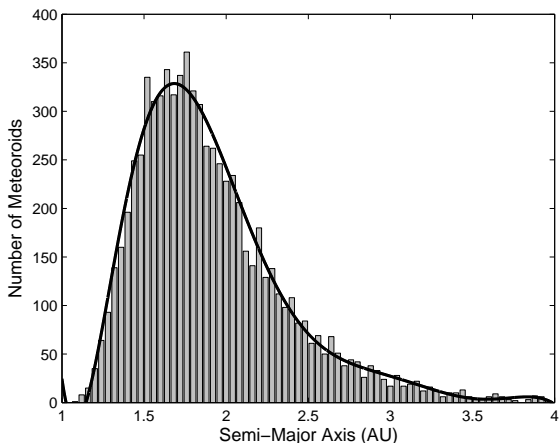### 6.1 Statistics of Variations from a Mean Curve

We first use a simple statistical test to determine whether the sizes of the small scale (less than ~ 0.5 AU) variations in the CMOR Taurid semi-major axis distribution are consistent with the size of the random fluctuations expected for this size of dataset. This involves fitting a model distribution to the data excluding the region in which the resonance centre is expected to be present. Our resulting dataset should not contain any signature of the resonance region. We obtain variations by subtraction of the model distribution and the data distribution. The standard deviation of these variations can then be compared with the size of the variations in the resonance region.

Ideally, a model of the physical underlying distribution would be used, including knowledge of observational biases. Since such a theoretical model is unknown, the actual model fit chosen is not a concern as long as it describes the data well: an eighth-order polynomial fit is chosen to model the underlying distribution of the data. Higher-order polynomials can produce non-monotonic behaviour or be overdetermined. Again, such issues are not of concern here provided the polynomial fits the data, particularly given that there is no attempt here to make predictions outside the data range. For the polynomials used here, undesirable behaviour can occur beyond the range over which the polynomial fitting is applying, but the eighth-order polynomial works well within the range of the data.

We create a semi-major axis histogram with a bin width equal to 0.04 AU. This is chosen as it is approximately the size of the resonant width for the 7:2 resonance and thus is approximately the expected size of the resonant feature. We remove an area around the expected location of the resonance in order to ensure any signature of the resonance does not bias the mean curve fit produced. In principle, the large measured uncertainties of the CMOR data will broaden such a resonant feature to cover a large area: this is further ad-
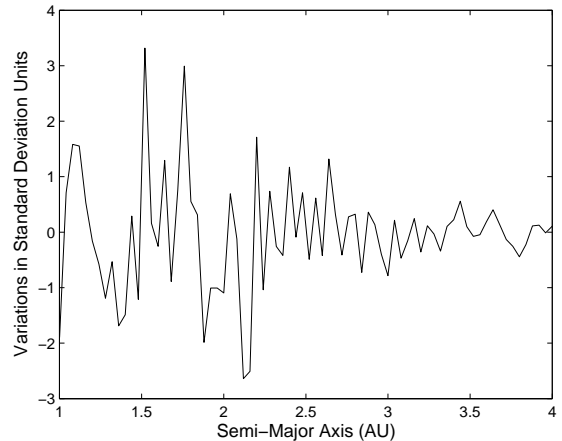
Figure 11. The variation of the standard deviation of the resulting variations as an increasing percentage of the data around 2.25 AU is removed.

Figure 12. *The observed CMOR Taurid data semi-major axis histogram, with the fitted eighth-order polynomial fit determined from the data (black line), but with the section 2.0-2.5 AU removed, as explained in the text.*

dressed in Section 9. The removed section is centred on the known resonance centre at 2.25AU.

It is necessary to remove the largest section possible around the resonance centre that still produces a satisfactory fit to the whole dataset. To test for the optimum number of data bins to remove, we monitor the fitting of the data using the standard deviation. We progressively remove an increasing set of points either side of the position of the resonance centre, and find that the fitting is good and the standard deviation steady up until the removal of about 14 data bins. After this point the fitting diverges from the data distribution, and the standard deviation begins to rapidly increase (see Figure 11). This is the result of removing in excess of 20% of the data points before completing the fitting. For this study the region 2.0 AU to 2.5 AU is removed (a total of 12 histogram bins: a safe choice below 14 points) before fitting an eighth-order polynomial to the histogram (see Figure 12).
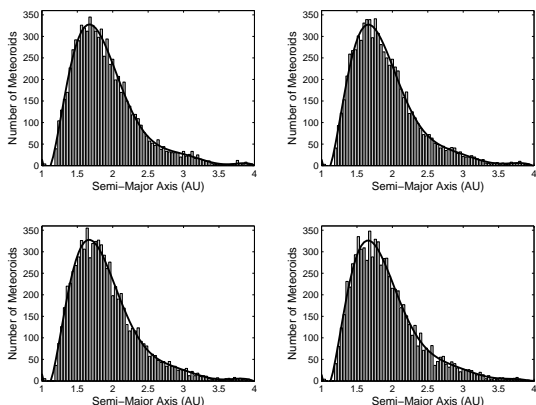

Figure 13. *The variations determined by subtraction of the CMOR data histogram bin numbers from the polynomial fitting to the reduced dataset.*

The variations between the polynomial fit and the CMOR data distribution (in units of standard deviation of the variations) are shown in Figure 13. Five peaks are observed at or above 1.95 standard deviations: in a statistically random distribution ~ 4 are expected, as 5% of fluctuations are expected to exceed 1.95 standard deviations. Similarly, there are 20 peaks above one standard deviation, and a statistically random distribution is expected to have ~ 24 (32%). While these numbers do not match exactly, they are within acceptable fluctuation ranges given the small number examined. This suggests the fluctuations in the CMOR data distribution have a random statistical origin. In particular, there is only one sample variation greater than two standard deviations in the region 2.0 AU to 2.5 AU (the region in which resonance indications are expected to be present). However, this feature is below the fitted curve (a variation of -2.64) and therefore is not evidence of a resonant peak. Moreover, there are fluctuations of this size in regions known not to contain a resonant swarm. These reasons allows us to disregard this feature as unrelated to our present problem. However, the resolution of the issue does benefit from an alternative approach: this is provided by the Monte Carlo method in the next section.

6.2 Monte Carlo Random Testing

The aim of this section is to determine whether a random selection of particles from the test distribution (an eighth-order polynomial) can, by chance, form features of the same level of significance as observed in the Taurid meteor data. This would suggest there is no evidence for a resonant feature in the current data.

We use a simple Monte Carlo method to select a random sample of semi-major axis values from a cumulative distribution created from an eighth-order polynomial model distribution. The result is a dataset of random meteors that is the same size as the original CMOR Taurid dataset (of 7649 meteoroids). This is used to produce a semi-major axis histogram (examples of which are seen in Figure 14) that can be compared with the CMOR Taurid distribution of
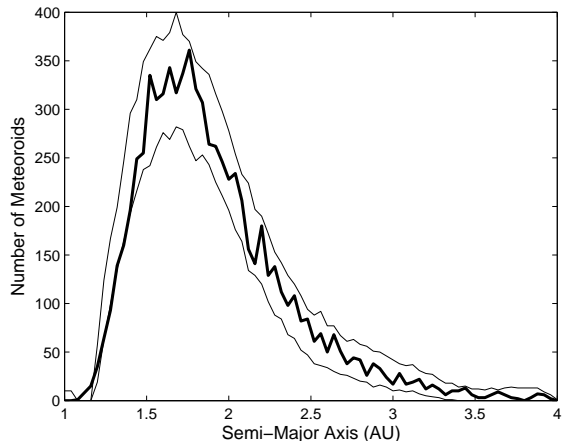
Figure 14. *Four examples of random selections of 7649 particles from an eighth-order polynomial distribution (shown as the overlying bold curve on each histogram). Note their similarly in appearance to Figure 12.*

Figure 15. *The maximum and minimum bin values (thin black lines) at each point here form a band inside which the majority of the CMOR Taurid semi-major axis histogram distribution (bold solid line) falls.*

Figure 12. Using the process of section 6.1, we determine the statistical fluctuations of this random distribution from a mean polynomial curve. In a very large dataset of semi-major axis values these variations would be close to zero, as there would be little or no statistical fluctuations. Thus, in this case the size of the variations determines the size of fluctuations from the mean curve that can be expected from statistics alone. If the residual fluctuations in the real data are of the same size as or lower than these variations, then it is possible to conclude that the fluctuations in the real data are statistically insignificant.

We create 600 such distributions of 7649 random meteor semi-major axis values. In order to compare the statistical fluctuations of the observed Taurid distribution and the random distributions from the Monte Carlo process, the number of variations in each dataset that exceed 2, 3 and 4 standard deviations are counted. For the observational CMOR data, 12 features are 2 standard deviations above the mean of the eighth-order polynomial fit, 3 exceed 3 standard deviations, and 2 exceed 4 standard deviations. For the artificial data, the average numbers of features (over the 600 datasets) exceeding 2, 3 and 4 standard deviations respectively are 12.12, 3.92 and 1.13. These values are in close agreement with those for the CMOR data.

A second simple test using these random datasets involves the simple maximum and minimum of the random datasets at each point. We produce 500 random distributions and calculate the maximum and minimum bin heights at each semi-major axis (see Figure 15). The CMOR data distribution falls within the maximum and minimum bounds produced by the random distributions, except at a sharp section with positive gradient ($a < 1.5$ AU). In this region the errors are a result of the poor fitting of the polynomial distribution. These errors are tolerated as this is not the region in which resonant signatures are expected. We therefore conclude that the CMOR data fluctuations can be produced by random distribution for at least the region $a > 1.5$ AU.

7 YEARLY VARIATIONS

Traditionally, the Taurid resonant swarm is investigated by comparison of data over several years. It is possible to compute a measure of the distance of the swarm from the Earth. This is given by ΔM, which is defined as the displacement in mean anomaly of the resonant centre from the point at which the Earth and swarm orbits cross in space and time. In years in which ΔM is small, significant increases in Taurid meteors numbers are expected due to the resonant swarm. Asher & Clube (1993) produce a list of such 'swarm encounter' years, defined as year for which $|\Delta M| < 40°$ on November 23 (the expected swarm encounter date). In the period of the CMOR observations used here, only 2005 is a 'swarm encounter' year. In this year $|\Delta M| < 11°$, which confirms that this is expected to be a good year for observations of this swarm: it is the closest November swarm encounter for 17 years.
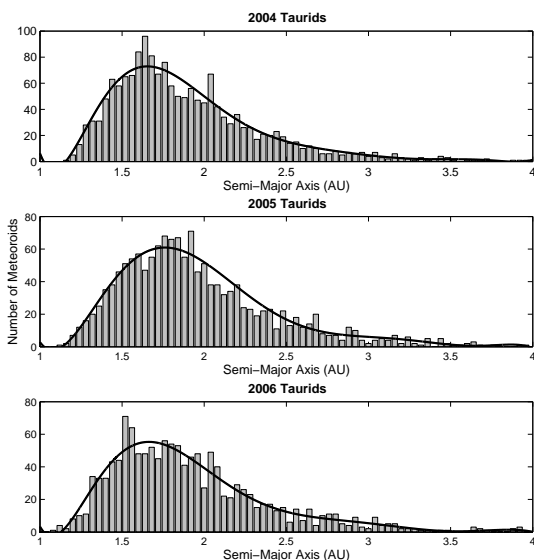
We therefore repeat the statistical analysis of Section 6.1 for the individual years 2002 to 2007, to determine whether there is any significant difference in the semi-major axis distribution of 2005 relative to non-swarm years. However, in contrast to the method given in this section, only five points either side of the resonant centre location are removed before a mean fit curve is produced. This is because the 2005 data produces unstable fittings for six or more points removed each side (see Section 6.1 for the test used to determine this). This is a consequence of the reduced size of the dataset.

The histograms and the resulting mean curves for 2004, 2005 and 2006 are displayed in Figure 16. Table 3 gives the number of features that are more than 1, 2 and 3 standard deviations above the mean curves for the years 2002 to 2007. We make two observations:

(i) The size of the data variations are nearly, but not exactly, consistent with the size expected for random statistical fluctuations. Histograms of the variations have a roughly Gaussian form. The numbers of features expected do not agree exactly with those given for 2005 in Table 3. However,

Year	# 1 std	# 2 std)	# 3 std
2002	18	6	1
2003	18	6	1
2004	15	6	2
2005	17	7	1
2006	17	6	1
2007	19	6	2
Approx. Expected Number	24	4	0 or 1

Table 3. *The number of features in excess of 1, 2 and 3 standard deviations for CMOR Taurid data for 2002-2006. Here '# 1 std' denotes the number of features that are more than 1 standard deviation away from the mean curve for that year. The final row gives the expected (comparison) numbers for the number of histogram bins used here drawn from the expected fluctuations in a random population.*

Figure 16. *Histograms and mean curve fittings for 2004, 2005 and 2006 CMOR Taurid data.*

the differences are not sufficient to conclude that there are significant differences between the variations observed and Gaussian random variations.

(ii) The data variations, as quantified in Table 3, are consistent between each year. There is no significant difference between the variations for 2005 and those for other (non-swarm encounter) years. Thus, there is no evidence of additional features due to the presence of the resonant swarm in 2005.

8   HIGHER QUALITY TAURID ORBITS

It is possible to extract higher quality orbits from the total CMOR Taurid dataset. These are the result of higher-precision velocity measurements made possible by the presence of Fresnel oscillations in the amplitude and phase of the meteor echo. Such echoes have $\leqslant 5\%$ speed errors instead of about $\leqslant 10\%$ (Jones et al. 2005), and should therefore

provide more reliable semi-major axis values. If the Fresnel oscillation pattern is sufficiently distinct (generally for meteors with a high signal-to-noise ratio), then both a time-delay speed and a hybrid Fresnel/pre-t_0 speed are achievable (see Hocking (2000) for further detail). Following Wiegert & Brown (2005), we form a new dataset containing only echoes for which a Fresnel/pre-t_0 speed is given, and for which the two speeds agree within 3%. The resulting dataset has 1025 meteors, 200 of which are from the year 2005. However, we find that neither the new dataset nor the meteors from 2005 in this dataset display evidence of the 7:2 resonant swarm: using the method given in Section 6.1 the variations of both datasets do not significantly exceed those expected as a result of random fluctuations (see Table 4).

As mentioned above, these meteors have in-atmosphere speed uncertainties of approximately $\leqslant 5\%$, as opposed to about $\leqslant 10\%$ for the time-delay speed method. Heliocentric velocity (V_H) uncertainties are related to semi-major axis (a) uncertainties by (Galligan 2000):

$$\left(\frac{\Delta a}{a}\right) = \frac{V_H^2}{1 - \frac{V_H^2}{2}} \left(\frac{\Delta V_H}{V_H}\right). \tag{7}$$

Here speeds are relative to the Earth's orbital speed, $GM_\odot = 1$, $R_E = 1$ and it is assumed that $r_h = 1$ AU. V_E and R_E are the velocity in space and the radius of the Earth, respectively; G is the gravitational constant and $M_\odot$ is the Solar mass.

The uncertainty in heliocentric velocity ΔV_H will include errors from several sources, most notably from errors in atmospheric deceleration calculations. Thus, it can be deduced that reducing the error in the in-atmosphere speed by a factor of two will reduce the semi-major axis uncertainties by not more than a factor of two. In Section 9 we see that such a reduction is not expected to allow us to resolve a resonant feature of the size expected.

Analysis therefore suggests that there is no evidence for a resonant swarm in CMOR-detected Taurids either in the combined datasets, in the 2005 dataset, or within higher quality orbits. This may indicate that the measurement uncertainties are too large for such small scale structure to be visible; or that the mass distribution of the swarm is such that there are few radar-sized particles in the swarm. We test the former in the following sections.

Year	# 1 std	# 2 std)	# 3 std
All Years	19	4	1
Approx. Expected Number All Data	24	4	0 or 1
2005	8	1	0
Approx. Expected Number 2005 Data	10	1 or 2	0

Table 4. *The number of features in excess of 1, 2 and 3 standard deviations for CMOR Taurid data for a restricted dataset containing higher-quality orbits, defined by echoes for which the time-lag and Fresnel/pre-t_0 velocities agree to 3%. Results are shown for the whole dataset, and for echoes from the year 2005 only. Here '# 1 std' denotes the number of features that are more than 1 standard deviation away from the mean curve for that year. Alternate rows gives the expected (comparison) numbers for the number of histogram bins used for each dataset.*

9 NUMERICAL STUDY OF OBSERVATIONAL UNCERTAINTIES

It is important to gain an understanding of what issues observational uncertainties may cause in the identification of any resonant peak. In particular, such uncertainties will broaden the Taurid semi-major axis distribution and individual resonant features. It is useful, therefore, to determine whether such features are detectable after they are broadened by the meteor radar orbital uncertainties, or what level of reduction in these uncertainties we require for such features to become significant. For this study the uncertainties we use are semi-major axis uncertainties. The results are applicable to velocity uncertainties also, as reducing the velocity uncertainties by a factor x will reduce the semi-major axis uncertainties by the same factor x (see equation 7).

Our method involves a 'convolution' (or, here, an addition) of:

(i) The overall distribution of non-resonant Taurids: This is modelled here by the observed Taurid distribution from the CMOR dataset. This may contain a small component of resonant swarm meteoroids, but this would make little difference to the results obtained, as it is seen above that the level of fluctuations from a random curve are consistent with the expected level of statistical fluctuations.

(ii) A modelled resonant peak: This is modelled by randomly selecting a number of meteoroids N_R from a Gaussian curve with the standard deviation equal to one quarter of the resonance width (determined to be ~ 0.047 in Section 5). This is because the full resonant width is equated with the 2σ 95% confidence section of the Gaussian distribution: the resonant width is defined as spaning 4σ across the Gaussian distribution. The number of meteoroids N_R injected into the swarm determines the height of the peak. We vary this as no information is available on the height of the resonant features in semi-major axis distributions. We will usually express this as a percentage of the total number of particles in the combined dataset. Here this is also called the 'resonant feature strength'.

(iii) The (assumed) Gaussian profiles for the uncertainty on each individual observed particle: We convert each data value from (i) and (ii) above from a point into a Gaussian profile in order to simulate the effect of uncertainties. We use the given semi-major axis uncertainties in the CMOR datasets for the standard deviations σ for each Gaussian profile. Each Gaussian is scaled to have an area of 1 under the curve.
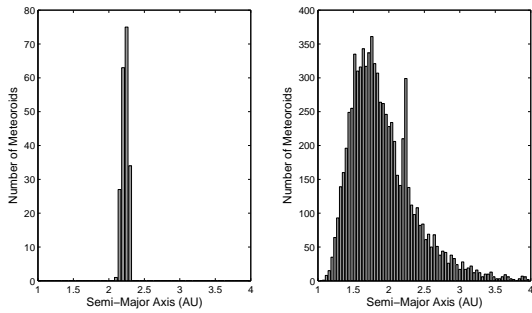
We conduct two separate tests using this model. The first assumes zero uncertainties and thus only combines distributions (i) and (ii) above. We use this 'perfect' data case to demonstrate the absolute lower size limit of a resonant feature that can be detected in a meteor radar dataset (of the size of the CMOR Taurid dataset used here). This is given in Section 9.2. The second test includes uncertainty broadening and thus all three distributions above are used. This test is given in Section 9.3.

The addition of uncertainty broadening can also be thought of as two distributions - the Taurid distribution and a model resonant feature - each composed of many individual Gaussians instead of many individual points (delta functions). This convolution is dealt with numerically by creating a histogram Gaussian to represent each point. Each Gaussian histogram meteoroid is defined from -4σ to $+4\sigma$, with steps of 0.04 AU (approximately the expected width of the resonance feature): thus, each meteoroid will cover a different number of bins depending on its corresponding uncertainty. The standard Gaussian formula is used:

$$G = \frac{1}{\sigma\sqrt{2\pi}} exp{-}(\frac{z^2}{2\sigma^2})$$

where z defines the size of the region covered by the Gaussian meteor in semi-major axis (-4σ to $+4\sigma$). By adding these Gaussian-broadened meteoroids we achieve a histogram of the semi-major axis distribution similar to that seen in Figure 12, but in which each meteoroid is fractionally split over several bins. We scale the resulting distribution in situations where the peak of the convolved distribution exceeds the peak of the original CMOR distribution. This is to ensure that the statistics remain comparable (to allow the standard deviation for the original dataset variations to be used: see Section 9.1).

Figure 17 shows a representative model resonant feature peak of 200 meteoroids (2.5%) randomly selected from the model Gaussian, and the complete distribution achieved by the addition of the fictitious resonant feature meteors to the Taurid dataset. Uncertainties are now applied to the combined dataset of Figure 17(b). We then determine whether the peak is statistically significant on application of uncertainty broadening. We can then vary the percentage or number of meteors in the swarm, which is unknown. We can also reduce the applied uncertainties by applying a fractional multiplication factor to the orbital uncertainties in the CMOR dataset.

Figure 17. *Model resonant features with $N_R = 200$ meteoroids in the resonance (that is, 2.4% of the total dataset are in the model resonant feature). The left figure demonstrates the selected peak alone, and the right figure its addition into the Taurid distribution.*

9.1 A Statistical Test

A statistical test is required to evaluate whether the resonant feature is statistically significant, both in the 'perfect' data case and in the uncertainty-broadened case. For consistency we use the first statistical test carried out on the CMOR data distribution (see Section 6.1). In summary, this involves:

(i) Removal of the resonant area of the distribution (approximately 2.0 AU to 2.5 AU)

(ii) Fitting of a test distribution to the remaining sections of the distribution

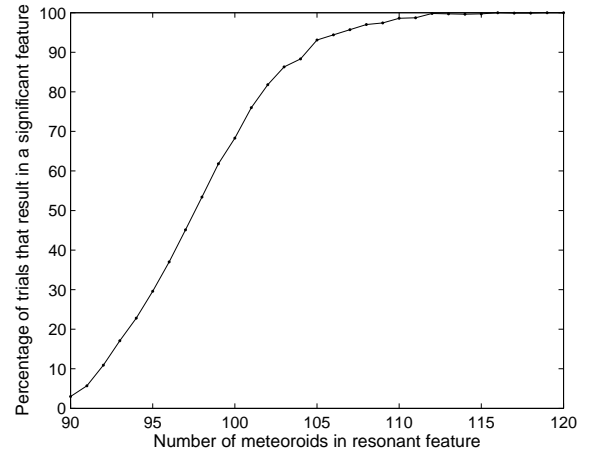(iii) Analysis of the variations between the distribution of interest and the fitted distribution

This was completed previously by comparing the variations (of (iii) in the statistical test summary) to the standard deviation of the variations themselves. Here we use the standard deviation of the variations of the original data distribution as the comparison value. This is because the uncertainty broadening will remove the small statistical fluctuations. Thus the statistical fluctuation information is contained only in the standard deviation of the variations of the original CMOR data.

By comparison with the statistical fluctuations in the CMOR data distribution, we conclude that a peak is considered significant if two conditions are fulfilled:
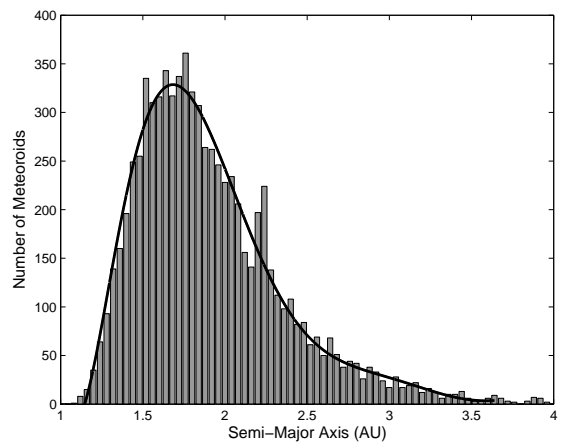
(i) The peak is above three standard deviations

(ii) Two adjacent points are above two standard deviations

The second condition is required because it is expected that these peaks will cover more than one histogram bin, and will not resemble the sharp statistical fluctuation features seen in Figure 13. We expect the feature to be a peak, not a trough, such that the variations should be positive if the distribution of interest is subtracted from the fitted distribution.

In addition, the model resonant peak involves a random element in the selection of particles from a Gaussian. This means that the decision as to whether a particular resonant feature peak size is significant may vary each time the process is run. Thus, we require a positive detection of the peak in 20 successive tests in order to conclude that the peak is statistically significant for that uncertainty level and peak size.

Figure 18. *The variation in the number of trials for which a significant peak is found, for a variety of fictitious resonant peak sizes. Above 112 meteoroids in the peak it can be seen that 99% of trials result in a significant peak.*
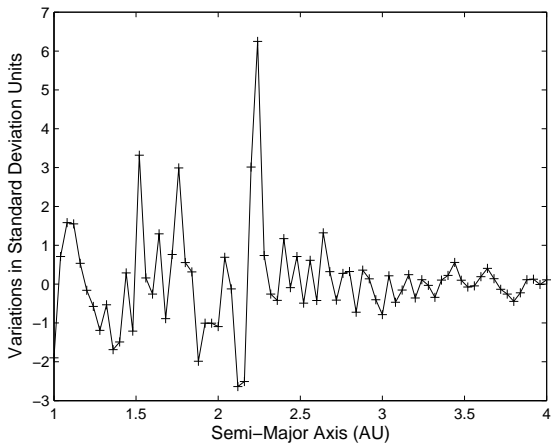

Figure 19. *The lowest resonant peak which is statistically significant for 'perfect' data (that is, data with no uncertainties) for 99% of trials is one with 112 meteoroids (1.4% of a dataset of this size). The combined semi-major axis distribution containing the CMOR Taurid data and the ficticious resonant peak is shown in (a), along with the eighth-order polynomial fit to the dataset (without the resonant region 2.0 to 2.5 AU).*

9.2 Perfect Data

Here we apply a statistical test to a 'perfect' dataset with a range of sizes for the test resonant peak. 'Perfect data' is defined here as data with no uncertainties or negligible uncertainties in the measured semi-major axis values: it is a consideration of the case in which statistical variations are larger than observational uncertainties. Therefore, no uncertainty broadening is included at this stage: only a resonant peak of a specific size (given by the number of particles in the peak) is added. We then use the above process to determine whether the resulting peak is statistically significant, and thus observable.

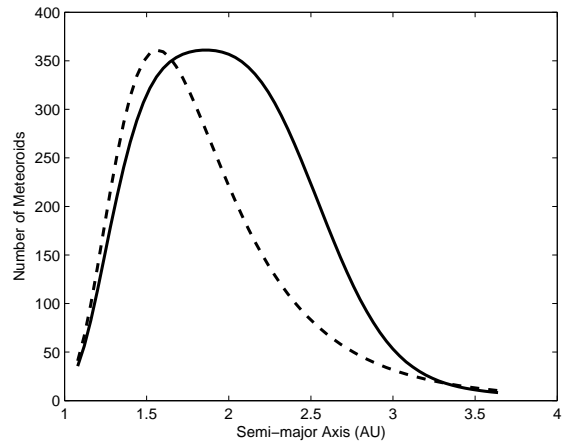We first run this test 20 times and determine the first

Figure 20. *The variations between the data histogram (with resonant peak) and polynomial fit distributions, scaled to the standard deviation of the variations of the original CMOR dataset.*

Figure 21. *The effect of high resonant feature particle numbers on the convolved dataset. An example of the behaviour of the numerical convolution at an uncertainty reduction factor of 2 at a resonant feature strength of 6000(44% of the total dataset). The distribution is dominated by the resonant feature. However, a statistical test would not be able to find evidence of a resonant feature unless the underlying Taurid distribution was known.*

peak size that is significant in all 20 tests. This is found to be a peak of 108 meteoroids: 1.39% of the total number of particles in the distribution (for a dataset of this size). This provides a result that can be compared with the uncertainty broadening case (Section 9.3). A higher accuracy test is then run, where this process is run 1000 times and the point at which 99% of trials result in a significant peak is determined (see Figure 18). An added resonant feature greater than or equal to 1.44% (112 meteoroids) fulfills this criterion. Additionally, any peak with size greater than 1.53% (119 meteoroids) produces significant features 100% of the time. We determine an uncertainty of 4 meteoroids from the difference between the limiting values determined in 20 and 1000 consecutive tests. Thus, $\sim (1.44 \pm 0.05)\%$ is the lower limit on the proportion of the stream that must be resonant in order for detection to be made by radar for this size of dataset. A distribution with a peak of this limiting size, and the variations from the polynomial fit are shown in Figure 19. Variations between the data histogram and the eighth-order polynomial are given in Figure 20.

9.3   Data with Varying Uncertainty Levels

Here we determine the approximate uncertainties (relative to those of CMOR) required of a meteor radar system for it to be capable of detecting a Taurid resonant swarm. This requires the addition of uncertainty broadening, as outlined in Section 9. To accomplish this we apply a range of fractional multiplicative factors to the uncertainty Gaussians based on CMOR uncertainties. We then determine which uncertainty levels result in statistically significant detections of the modelled resonant peak, for a range of sizes for this peak.

   The range of integer-value 'uncertainty reduction factors' from three to fourteen are explored. These factors represent values by which the uncertainties are divided: that is, an 'uncertainty reduction factor' of 3 represents a reduction in the uncertainties to $\frac{1}{3}$ of their original values. An uncertainty reduction factor of 2 requires an unrealistically large number of particles in the resonant swarm for a statistically significant peak to be observed. Therefore, e do not include
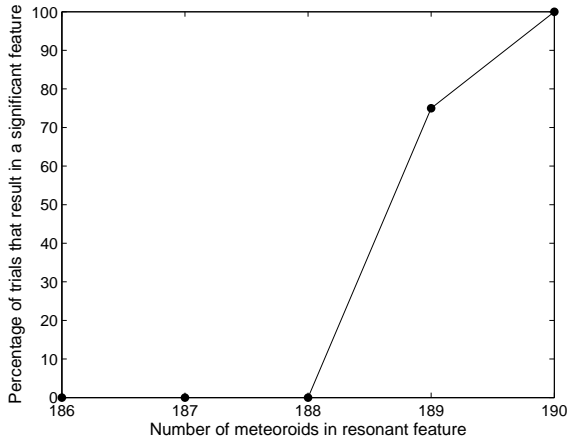
uncertainty reduction factors less than 3. Furthermore, we find that the method is less robust after the modelled resonant swarm comprises $\sim 40\%$ to 50% of the total dataset, as after this point the convolution starts to move the peak of the distribution away from the Sun (see Figure 21). However, the percentage of the total number of Taurid particles that are in the 7:2 Taurid resonant swarm is unlikely to be higher than 40% (see below). If this method were to be applied in a situation where a swarm may comprise more that 50% of the total dataset, use of this numerical convolution would require a different model for the overall distribution of non-resonant Taurids.
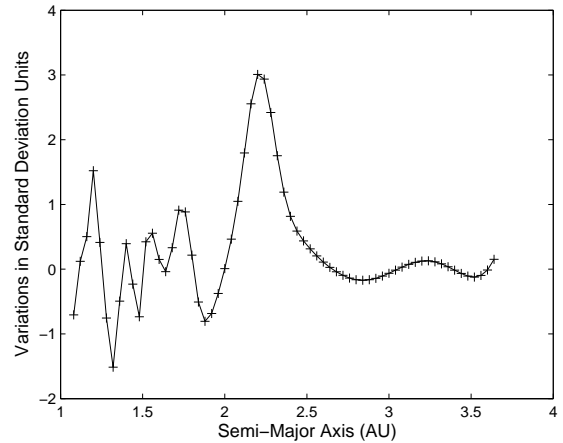
   This restriction also implies that an uncertainty reduction factor of 1 (that is, no change to the current uncertainties) will not result in a significant detection of the resonant swarm, unless more than 50% of observed Taurids are resonant, which is unlikely. Thus, broadening as a result of the uncertainties of the CMOR dataset will not allow observation of the Taurid resonant swarm.

   For uncertainty reduction factor values greater than fourteen the method reaches its limitation as the uncertainties begin to become smaller than the histogram bin size used. This only affects the smallest semi-major axis values at first (with the lowest absolute uncertainties), but will affect the whole distribution for very high uncertainty reduction factor values. An improved algorithm would be able to deal with this situation. However, given that by a reduction factor of 14 the resonant feature values required for significance are close to those required in the 'perfect' case, this is not pursued here.
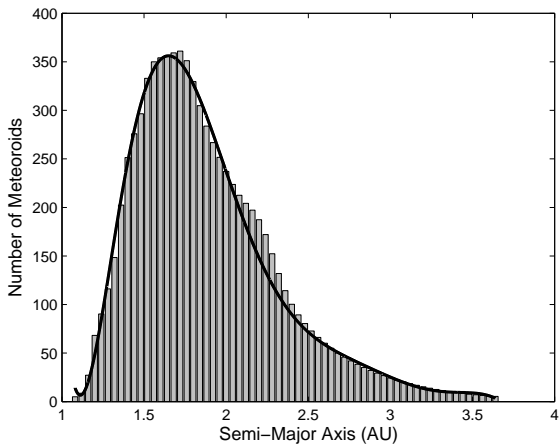
   For each uncertainty reduction factor we determine the minimum modelled resonant peak size required. The method for this is given in Section 9.1. Uncertainties are given by the difference in resonant peak size between a size for which $\frac{1}{20}$ tests provide a statistically significant result, and one that allows $\frac{20}{20}$ to pass. This is usually a maximum of ~ 3 meteoroids, though in some cases it is 1 meteoroid or less. As

Figure 22. *The variation in the number of trials for which a significant peak is found, for a variety of fictitious resonant peak sizes, and at an uncertainty reduction factor of 9. Above 190 meteoroids in the peak it can be seen that 100% of the 20 consecutive trials resulted in a significant peak.*
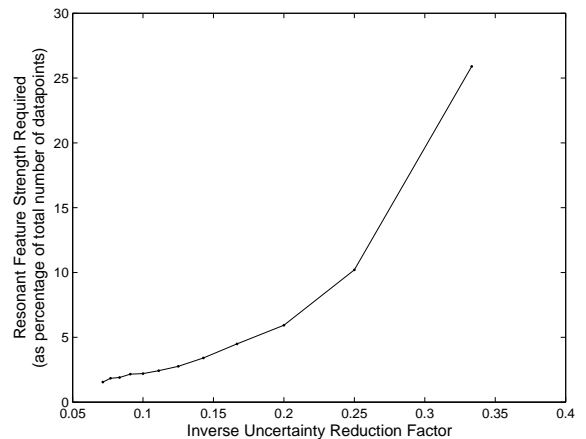

Figure 24. *The variations between the data histogram (with resonant peak) and polynomial fit distributions, scaled to the standard deviation of the variations of the original CMOR dataset, for a feature with 190 meteoroids (2.4% of a dataset of this size), with an uncertainty ±3 meteoroids.*

Figure 23. *The lowest resonant peak which is statistically significant in 100% of 20 trials for uncertainty broadened data with an 'uncertainty reduction factor' of 9. This is a feature with 190 meteoroids (2.4% of a dataset of this size), with an uncertainty ±3 meteoroids. The combined semi-major axis distribution containing the CMOR Taurid data and the ficticious resonant peak, both uncertainty broadened, is shown along with the eighth-order polynomial fit to the dataset (without the resonant region 2.0 to 2.5 AU).*

Figure 25. *The resonant feature strength detectable for each inverse uncertainty reduction factor. For example, a reduction in uncertainty by a factor of about 9 (or inverse 0.11, which is the fraction by which CMOR uncertainties must be multiplied) is required to observe a resonant feature with 200 particles (2.6% of the dataset).*

an example, this is demonstrated using the size of the resonant feature required at an uncertainty reduction factor of 9. Figure 22 shows the percentage of tests that produce a significant result for resonant feature sizes of 2.37% to 2.42% (equivalent to 186 to 190 particles for an initial dataset of 7649 meteoroids). The minimum significant resonant feature size for which all 20 tests produce a significant result is 2.42% (190 meteoroids). The uncertainty is 1 meteoroid (or 0.013% of this total dataset), as only one 'resonant feature size' below 190 meteoroids can produce a significant result (see Figure 22). The resulting broadened distribution and variations from the mean curve are given in Figures 23 and

24. In particular, it is interesting to note the broad, smooth form of the variations in Figure 24 compared with those for the 'perfect' data case in Figure 20. We recognise that these uncertainties will be larger as a result of the limitation of using the current CMOR Taurid distribution in the method. This is difficult to quantify but is addressed to some extent in Section 9.5.

Figure 25 shows the resonant feature strengths that are observable for a given reduction in the radar uncertainties. This figure can be used either to determine the required minimum uncertainty reduction factor for a CMOR type radar for a given resonant feature size; or to determine the required minimum resonant feature size for a given level of uncertainty reduction.

The values given in Figure 25 are only valid for the size of CMOR dataset used here. An uncertainty reduction factor of 14 will allow a swarm of a similar size to be detected as for the perfect data (120 meteoroids for a reduction in uncertainties of 14; and 108 for a 'perfect' data). This implies that a limit is reached by the radar uncertainties: after a reduction in uncertainties of 12 to 14 statistical variations will largely govern the visibility of resonant swarms, and further improvement in the radar will not assist greatly in detection. This study, and the 'perfect' data study, thus imply that for radar datasets of this size, swarms which comprise less than $\sim 1.5\%$ of the meteoroid stream are unlikely to be detectable using this methodology, regardless of the uncertainties of the radar system.

Therefore, for a radar dataset of this size, and with the requirement that resonant meteoroids comprise more than $\sim 2\%$ of the radar Taurid dataset, a radar with improvement in uncertainties given by a reduction factor of 12 or higher (equivalent to 8% of the current uncertainties) should be able to detect a resonant swarm in Taurid meteoroids (assuming that the radar system has approximately the same mass sensitivity as CMOR). A resonant peak that is 2.2% of the number of Taurids in the dataset should be detectable by reducing CMOR uncertainties by a factor of 10. Such an enhancement is considered feasible with the current techniques of radar systems and signal processing.

9.4 Visual Data on Taurids

The uncertainty reduction levels considered above require knowledge of the approximate proportion of Taurids that are resonant. This is difficult to determine, and is dependent on the location of the swarm with respect to the Earth, the number of particles in the swarm and the size distribution of these particles. Since few radar observations of the Taurid swarm exist, we must use visual observations to obtain estimates of the size of the resonant swarm. Results from visual meteoroid studies will only be applicable to radar data if the number of radar-sized particles in the swarm is similar to the number of visual particles.

We use the activity profile (of ZHR as a function of solar longitude) for visual Taurids of 2005 given in Dubietis & Arlt (2007) to estimate the maximum proportion of 2005 Taurids that are resonant. ZHR is an indicator of particle numbers: an actual mass flux is dependent on the population index. However, Dubietis & Arlt (2007) find that the population index of visual Taurids is roughly constant, fluctuating around a population index of 2.4. We use simple area calculations to determine the approximate number of meteoroids in the 2005 profile, compared with the number of meteoroids in a typical annual profile averaged over 1985-2004. We find that the enhanced 'swarm' region of the profile (the region that differs markedly from the typical annual profile) contains $\sim 30\%$ of the meteoroids contained in the total 2005 profile. For 1988 and 1998 this provides 23% and 41% respectively. These values cannot be considered highly accurate, and are only indicative. The three years tested here represent optimal years for swarm detection, with the mean longitude of the resonant centre of the swarm being within $15°$ of the mean longitude of the Earth. However, the proportion of swarm meteoroids and maximal ZHR values (calculated by Dubietis & Arlt (2007)) are not well corre-lated with the proximity of the swarm to the Earth. This is still an issue after consideration of the presence of a full moon in some years - particularly in 1995 and 1998. This could reflect other variations in observational geometry of the swarm.

Additionally, the proportion of swarm particles detected by visual methods may be larger than that detected by radar methods, because it is possible that larger particles are more easily trapped in the resonance if ejected from a resonant or near-resonant comet (such as is observed for Leonid meteoroids (Jenniskens & Betlem 2000)). This may depend on the ejection mechanism for the Taurid resonant particles.

For these reasons we cannot be precise here on the expected proportion of swarm particles in radar datasets. In general, however, we expect that the proportion of particles will not exceed 20–30% of the total dataset for a swarm year. This is equivalent to ~ 5–8% of the total CMOR dataset spanning the years 2002–2007.
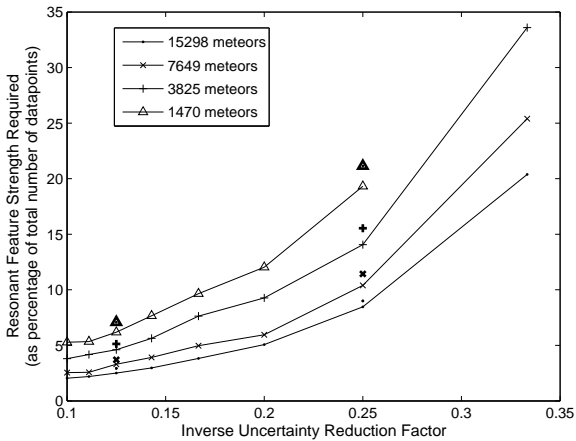
9.5 Variation with the Dataset Size

Here we determine the variation of the results of Section 9.3 as a function of the size of the dataset. This serves two purposes here: (i) to determine the effect if an improved radar is operated for a shorter or longer time than the 2002–2007 period producing the CMOR dataset used here; and (ii) to determine the required number of particles in any one year required to produce a statistically significant result for a given reduction in uncertainties.

These aims require modifications to be made to the numerical method given in Section 9. To obtain a representative dataset that has the same distribution shape as the CMOR Taurid semi-major axis distribution, but is composed of a different number of particles, we employ the Monte-Carlo method given in Section 6.2. This allows the random selection of a given number of particles from an eighth-order polynomial fit to the CMOR Taurid semi-major axis distribution. We calculate a standard deviation of the variations between the random dataset and this fitted curve in order to perform the statistical test given in Section 9.1. The uncertainty values for each semi-major axis are determined using a quadratic fitting to the CMOR data uncertainties, which provides the uncertainty as a function of semi-major axis. We add a random component to each uncertainty to model the scatter in uncertainty values, again using a fitting to the CMOR data. The remainder of the methodology is identical to that used in Section 9. Due to the fact that the distribution is now randomly produced, the uncertainty levels will be much higher than previously (where only the model resonant feature was produced randomly). However, this modified method is more robust as it accounts for the variations in the statistical fluctuations that can occur, whereas the results of Section 9.3 depend on the statistical fluctuations of an improved dataset being the same as those in the current CMOR Taurid dataset.

We choose four sizes of test datasets:

(i) the size of the CMOR dataset used here (7469 meteors)
(ii) half the size of the CMOR dataset (3825 meteors)
(iii) double the size of the CMOR dataset (15298 meteors)
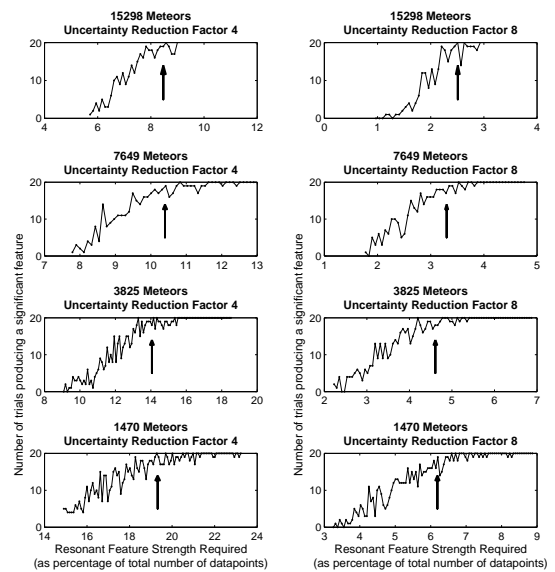(iv) the size of the CMOR dataset for 2005 (1470 meteors)

Figure 26. *The variation in the size of the resonant peak (as a percentage of the size of the total dataset) required for a statistically significant detection at each level of uncertainty reduction, relative to the CMOR uncertainties of the current dataset. Each line shows a different number of particles in the source dataset. The lower three lines (15298, 7649 and 3825 meteors) represent datasets of double, equal and half the size of the CMOR dataset used in this chapter. The upper line (1470 meteors) represents the number of particles detected in the 2005 swarm year by CMOR: that is, this provides the approximate percentages of meteoroids that must be in the observable radar Taurid stream in order for detection to be made based only on one year of data. This is important given that the swarm's location relative to the Earth is only optimal for observation every 3 to 5 years. The bold points above the curves demonstrate the resonant feature strengths required for a 95% probability of a significant detection of the resonant swarm for a given uncertainty reduction factor and dataset size.*

The final dataset size is important as it provides the requirements for detection of the swarm in one year of data. This is necessary because the swarm is only in a good location for observation relative to the Earth once every 3 to 5 years (see Section 7).

For each dataset, and for each integer-value uncertainty reduction factor of 3 to 10, we find the first resonant feature strength that produces 20 consecutive significant tests (see Figure 26). Figure 26 identifies the approximate resonant feature size that can be observed for a given uncertainty in meteor radar semi-major axis data. It can also provide the approximate uncertainty reduction required in order to detect a feature of a given size. As expected, a smaller dataset requires a larger resonant feature for significant detection to be made. However, the differences in the required resonant feature strength are not as large as the differences in the size of the dataset. For example, case (iii) only decreases the size of the resonant feature required by 15–25% compared to case (i). Similarly, case (ii) produce significant detection of a resonant feature 25–40% larger than case (i).

As mentioned above, there will be significant fluctuations in the results due to the random element of the method. This error is evaluated by testing a region around a number of the points on Figure 26. For each dataset size, for uncertainty reduction factors of 4 and 8, we test between 50 and 100 resonant feature strength values (in steps of 5 or 10) either side of those resonant strength values given in

Figure 27. *The number of tests resulting in a significant resonant feature for each resonant feature strength at datasets of sizes 1470, 3825, 7649 and 15298, for uncertainty reduction factors 4 and 8. Arrows on each graph indicate the values of resonant feature strength plotted on Figure 26.*

Figure 26. Again, we run 20 tests for each set of values. In Figure 27 the number of tests out of 20 that produce a significant result for each resonant feature strength is plotted. The resonant feature strength values used to produce Figure 26 are indicated by arrows on each graph. It is evident that the values given in Figure 26 refer to the resonant features strengths that will in all but two cases provide a greater than 80% chance of detecting a significant feature. The two exceptions are for datasets of size 15298 and 1470 meteors, with uncertainty reduction factor 8: in these cases there is a greater than 70% of detecting a significant feature. In both cases an increase in the resonant feature size of less than 5% would produce a greater than 80% chance of sucess.

The resonant feature strength (for each uncertainty reduction factor) that would allow a significant detection of the resonant feature in 95% (19 out of 20) of cases is also of interest. It is at this level of confidence that we expect a radar with such an orbital measurement uncertainty (or uncertainty reduction) to be able to detect a swarm of that resonant feature size. For an uncertainty reduction factor of 4, values $\sim 10\%$ greater than those in Figure 26 are required to achieve a significant resonant peak in 95% of cases. For an uncertainty reduction factor of 8, values 11–17% greater are required. The bold points in Figure 26 demonstrate the 10–17% improvement in the results required to provide a 95% probability of detecting the resonant swarm in the given values.

If one year of data from a swarm close-approach year is available, then the expected proportion of resonant swarm particles will be higher than in a general dataset: it may be as high as 20–30% for a strong swarm encounter year (see Section 9.3). If this is the case, it is possible that a radar with an improvement of measurement uncertainties of only a factor of 4–5 could detect this resonant swarm (see

Figure 26). The required improvement in uncertainties will depend on whether there are approximately the same number of radar-sized swarm particles as visual-sized particles. However, as long as the resonant swarm results in a 5–6% increase in radar-sized particles, a radar with uncertainties one tenth of those of the CMOR dataset used here should be capable of detecting the swarm.

10   SUMMARY AND CONCLUSIONS

The detection of a meteoroid resonance swarm with a radar system requires improvement of the orbital uncertainties. In this work we find no evidence for the 7:2 Taurid resonance swarm in CMOR data, which should theoretically be amongst the most easily-observed resonance effects in radar data (see Section 3). In addition, the uncertainties of the CMOR dataset used here (which are typical of current systems) are too large to allow observation of the resonant swarm. The level of improvement required is highly dependent on the size of the resonant swarm, and the resulting increase in the number of Taurid particles observed in a swarm year. If the resonant swarm comprises 20–30% of resonant particles in a swarm year, then potentially one year of observations with a meteor orbit radar with orbital uncertainties a factor of 5 lower than CMOR could detect the swarm; however, if the swarm comprises only 5–6% of the total Taurids, a factor of 10 improvement in the radar uncertainties would be required. These factors of reduction in semi-major axis uncertainties are equivalent to the required reduction factors for the velocity uncertainties. The size of the swarm that can be observed is found to plateau after an improvement in orbital uncertainties of a factor of ~ 10 (see Figure 25). At this point a swarm consisting of $\sim 5\%$ of the Taurid dataset would be observable in about one year of radar data. Therefore, improvements above a factor of 10 are not likely to greatly improve the chance of observing a resonant swarm.

Such improvements in meteor radar measurement uncertainties, though they present technical difficulties, may be feasible with current techniques of radar systems and signal processing. In particular, the addition of more stations and with the ability to recover phase information and interferometry from multiple stations would produce an overconstrained system of equations for speed/trajectory determination. These would allow calculation of the deceleration of meteors in the Earth's atmosphere, and would significantly improve the velocity uncertainties for detected particles. This approach is the motivation behind an improved CMOR II radar which will have five remote stations in addition to the home site (Brown et al. 2010). Higher sampling rates (achieved by an improvement in the pulse repetition frequency) would also improve orbital uncertainties. The Fresnel velocity method can provide a factor of ~ 2 improvement in the velocity uncertainties in comparison to the time-delay method (see Section 8). An additional important method of determining meteoroid velocities is the Fresnel transform method, developed by Elford (2001). This method is capable of producing speeds with precision of ~ 0.1 km^{-1}, compared with uncertainties of ~ 3 kms^{-1} for a 30 kms^{-1} meteor with the time-delay method: equivalent to a 10% velocity uncertainty (Baggaley & Grant 2004). However, it is limited to use for meteors with high signal-to-noise ratios. It is therefore expected that improvement of deceleration calculations provides the greatest chance of reaching the required accuracy for detection of resonant structures.

REFERENCES

Asher D. J., Clube S. V. M., 1993, Quarterly Journal of the Royal Astronomical Society, 34, 481

Asher D. J., Clube S. V. M., 1998, Celestial Mechanics and Dynamical Astronomy, 69, 149

Asher D. J., Clube S. V. M., Steel D. I., 1993, in Meteoroids and their Parent Bodies The Taurid complex asteroids

Asher D. J., Emel'yanenko V. V., 2002, Monthly Notices of the Royal Astronomical Society, 331, 126

Baggaley W. J., Grant J., 2004, Earth, Moon, and Planets, 95, 601

Brown P., Jones J., Weryk R. J., Campbell-Brown M. D., 2004, Earth, Moon and Planets, 95, 617

Brown P., Weryk R. J., Wong D. K., Jones J., 2008, Icarus, 195, 317

Brown P., Wong D. K., Weryk R. J., Wiegert P., 2010, Icarus, 207, 66

Clube S. V. M., Napier W. M., 1984, Monthly Notices of the Royal Astronomical Society, 211, 953

Dubietis A., Arlt A., 2007, Monthly Notices of the Royal Astronomical Society, 376, 890

Elford W. G., 2001, in Proceedings of the Meteoroids 2001 Conference Observations of the structure of meteor trails at radio wavelengths using fresnel holography. pp 405 – 411

Emel'yanenko V. V., 2001a, in Proceedings of the Meteoroids 2001 Conference, Swedish Institute of Space Physics, Kirunda, Sweden, 6-10 August 2001 Resonance structure of meteoroid streams. pp 43–45

Emel'yanenko V. V., 2001b, in Proceedings of the Meteoroids 2001 Conference Resonance structure of meteoroid streams. Sweedish Institute of Space Physics

Gallardo T., 2006, Icarus, 184, 29

Galligan D. P., 2000, PhD thesis, University of Canterbury

Hocking W. K., 2000, Radio Science, 35, 1205

Hocking W. K., Fuller B., Vandepeer B., 2001, Radio Science, 63, 155

Jenniskens P., 2006, Meteor Showers and their Parent Comets. Cambridge University Press

Jenniskens P., Betlem H., 2000, The Astrophysical Journal, 531, 1161

Jenniskens P., et al., 1998, Monthly Notices of the Royal Astronomical Society, 301, 941

Jones J., Brown P., Ellis K. J., Webster A. R., Campbell-Brown M., Krezemenski Z., Weryk R. J., 2005, Planetary and Space Science, 53, 413

Murad E., Williams I. P., eds, 2002, Meteors in the Earth's Atmosphere. Cambridge University Press

Murray C. D., Dermott S. F., 1999, Solar System Dynamics. Cambridge University Press

Rauch K. P., Hamilton D. P., 2002, Bulletin of the American Astronomical Society, 34

Rendtel J., 2008, Earth, Moon and Planets, 102, 103

Roy A. E., 1988, Orbital Motion. A. Hilger

Ryabova G. O., 2005, in Lazzaro D F. M., A F. J., eds, Proceedings of Asteroids, Comets, Meteors, IAU Symposium No. 229 Meteoroid streams: mathematical modelling and observations. pp 229–247

Sato M., Watanabe J., 2007, Publication of the Astronomical Society of Japan, 59, L21

Spurný P., Shrbený L., 2008, Earth, Moon and Planets, 102, 141

Steel D. I., Asher D. J., Clube S. V. M., 1991, Monthly Notices of the Royal Astronomical Society, 251, 632

Trigo-Rodríguez J. M., Madiedo J. M., Llorca J., Gural P. S., Pujols P., Tezel T., 2007, Monthly Notices of the Royal Astronomical Society, 380, 126

Valsecchi G. B., Morbidelli A., Gonczi R., Farinella P., Froeschlé C., Froeschlé C., 1995, Icarus, 118, 169

Wiegert P., Brown P., 2005, Icarus, 179, 139

This paper has been typeset from a TEX/ LATEX file prepared by the author.